Enhanced Wind Farm Performance via Active Wake Control

A Steady-State Approach

Dammann, Tim; Van Der Hoek, Daan; Yu, Wei; Van Wingerden, Jan Willem

DOI
10.23919/ACC63710.2025.11107695

Publication date
2025

Document Version
Final published version

Published in
Proceedings of the American Control Conference, ACC 2025

2025 American Control Conference (ACC)
July 8-10, 2025. Denver, CO, USA

Enhanced Wind Farm Performance via Active Wake Control: A Steady-State Approach

Tim Dammann[1], Daan van der Hoek[1], Wei Yu[2], and Jan-Willem van Wingerden[1]

Abstract— **Denser turbine spacing in wind farms leads to increased wake interactions, causing power losses when each turbine operates under its own greedy control scheme. To mitigate these effects, research is exploring strategies that consider the entire wind farm rather than singular turbines. The so-called helix approach has recently gotten significant attention from the research community. It aims to reduce wake losses through periodic individual pitch control. Wake steering on the other hand uses yaw actuation to laterally deflect the wake away from downstream turbines. In this paper, we adapt and validate a steady-state surrogate model to compute the time-averaged velocity field behind a wind turbine operating with the helix approach. The model is tuned using data from Large Eddy Simulations. We compare the helix model to wake steering and baseline operation in a wind farm case study, demonstrating that the helix approach offers promising benefits under specific wind conditions.**

I. Introduction

With the increase of global wind energy capacities, it has become common practice to cluster wind turbines in wind farms to save on installation costs and maximize power extraction in areas of beneficial wind conditions. However, when wind turbines extract kinetic energy from the wind, they cause a velocity deficit behind their rotor, known as the wake, which negatively impacts the power production of downstream turbines. Conventional wind turbine control strategies focus on maximizing the power production of singular turbines, which results in a stronger velocity deficit behind the turbine. Despite being beneficial for a single turbine, this approach is suboptimal when considering the power production of a whole cluster. As a result, wind farm control strategies have been developed to minimize wake losses while still ensuring high energy extraction [1].

One widely studied form of wind farm control is wake steering control, in which a turbine uses its yaw actuators to slightly misalign itself with the incoming wind direction, causing a deflection in the wake behind the rotor. By doing so, the wake can be steered away from downstream turbines, as demonstrated in the development of wake steering control schemes [2]. Procedures for finding optimal yaw offsets under dynamic wind conditions have also been explored [3], and field tests have validated the effectiveness of wake steering in real-world applications [4].

Recently, wake mixing control has gained significant attention from the research community, with various control strategies investigated [1]. One promising approach, known as the helix method [5], addresses issues like high power and load fluctuations observed in other strategies such as dynamic induction control, while achieving substantial cumulative power gains [6]. This method employs dynamic individual pitch control, which was previously mainly used for load mitigation [7], [8], to create a helical wake deflection, enhancing mixing with free stream velocity and accelerating wake recovery. However, recent studies have shown that while the Helix approach is able to increase power production, certain controller settings may also lead to higher pitch bearing damage and turbine loads [9]. To further investigate the scaling between control input and resulting power gains, Large Eddy Simulations (LES) were used to explore the impact of varying helix amplitudes, demonstrating a continuous increase in power output up to a six-degree pitch amplitude while identifying a threshold for effective wake recovery and an upper limit due to turbine loading [10]. In [11], the physical mechanisms behind the increased power production of the helix approach, along with the synchronization of the helix phase in a three-turbine array, were examined. The study found that in a multi-turbine configuration, the helix phase offset plays a critical role in optimizing power output.

In the aforementioned studies, the helix approach has always been simulated through LES employing an Actuator Line Method (ALM) to simulate the varying pitch angle of individual turbine blades. While offering high accuracy, LES-ALM simulations come with high computational costs, limiting the simulations to a small number of turbines. When considering large wind farms, this approach is no longer feasible. Therefore, this study will implement commonly used engineering models to replicate the time-averaged velocity field behind a turbine when the helix is employed. With this approach, we can study the effect of the helix approach on the power production of a wind farm for different ambient conditions. Furthermore, we compare the increase in power production with the helix approach to wake steering.

II. Steady-State Helix Surrogate Model

The steady-state helix surrogate model used in this work combines a single wake velocity deficit model as described in [12], which we tuned to high fidelity data, with a blockage deficit model according to [13], and a turbine-induced turbulence model following [14]. The wakes of different turbines are summed up linearly. A steady-state helix surrogate model has been implemented in the FLOw Redirection and Induction in Steady State (FLORIS) framework [15]; however, this

[1]Delft Center for Systems and Control, Faculty of Mechanical Engineering, Delft University of Technology, Delft, The Netherlands. [2]Wind Energy Section, Department of Flow Physics and Technology, Faculty of Aerospace Engineering, Delft University of Technology, Delft, The Netherlands, {T.Dammann, D.C.VanDerHoek, J.W.vanWingerden, W.Yu}@tudelft.nl.

study develops a novel steady-state surrogate model within the *PyWake* framework to enhance compatibility with high-fidelity data and better capture wake dynamics. For wake steering operation, the wake deflection and redirection model from [16] was applied. The velocity used to calculate the turbine power, wake deficit and added turbulence is obtained using 21 points across the rotor plane according to [17]. The single wake model from [12] was chosen based on a high agreement with the high fidelity data as described in Section III. The different engineering models were all combined under the umbrella framework *PyWake* [18], an open-source framework developed by the Technical University of Denmark that combines different engineering wake models with the aim of calculating the Annual Energy Production (AEP) of a wind farm. To represent the next generation of offshore wind turbines, the IEA-22MW reference wind turbine [19] was selected for this case study. The turbine has a rotor diameter of $D = 283.2\,\mathrm{m}$ and a rated power of $P_{rated} = 22\,\mathrm{MW}$. A model for the IEA-22MW turbine in PyWake was created based on turbulence dependent thrust and power coefficients obtained with OpenFAST [20], which is a widely used aeroelastic simulation tool for wind turbines. The turbulence was generated according to the IEC Kaimal spectrum, using the TurbSim Software [21].

The steady-state wake model computes the velocity deficit behind the turbine as a product of the maximum velocity deficit $C(\tilde{x})$ and a shape function $f(\tilde{r})$, with $\tilde{x}, \tilde{\sigma}$, and $\tilde{r}$, the axial distance from the turbine, the characteristic wake width, and the radial distance from the wake center, respectively, normalized by the turbine diameter d_0:

$$\frac{U_\infty - U_\mathrm{w}}{U_\infty} = C(\tilde{x}) f(\tilde{r}) = C(\tilde{x}) e^{-\tilde{r}^n/\left(2\tilde{\sigma}^2\right)}. \tag{1}$$

Here, U_∞ denotes the freestream velocity, and U_w is the velocity in the wake. The maximum velocity deficit $C(x)$ is defined as:

$$C(x) = 2^{2/n-1} - \sqrt{2^{4/n-2} - \frac{nC_T}{16\Gamma(2/n)\sigma^{4/n}}}, \tag{2}$$

in which n denotes the Super Gaussian Order and Γ a parameter, which recovers the original form of $C(\tilde{x})$ as proposed by Bastankah and Porté-Agel [22] when $\Gamma(1) = 1$ and $n = 2$. The characteristic wake width (σ) is a function of the turbulence intensity, according to:

$$\sigma = (a_s T_i + b_s)x + c_s\sqrt{\beta}, \tag{3}$$

with β a function of the thrust coefficient C_T of the turbine:

$$\beta = \frac{1}{2}\frac{1+\sqrt{1-C_T}}{\sqrt{1-C_T}}. \tag{4}$$

Finally, the analytical super Gaussian parameter n is defined as:

$$n = a_f e^{b_f x} + c_f, \tag{5}$$

in which the parameters $(a_s, b_s, c_s, a_f, b_f, c_f)$ represent calibration parameters, which will be fitted to the LES data in Section III.

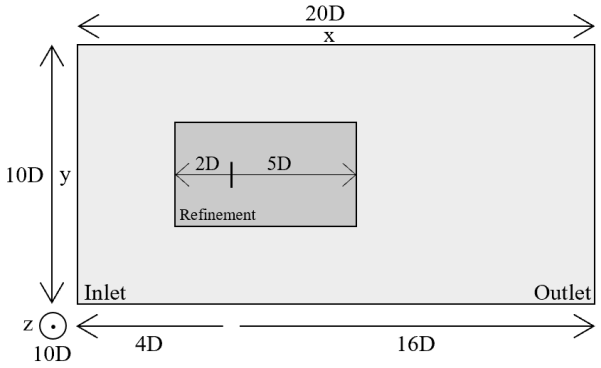

Fig. 1: Sketch of the LES domain. The length of the domain is $20D$ in streamwise direction and 10D in both lateral directions. The turbine rotor is placed at a distance of 4D from the inlet.

III. High Fidelity Model

For this work, several LES were conducted with the IEA-22MW turbine to generate data for model calibration and validation. All simulations were performed with the simulation tool AMR-wind, developed by the National Renewable Energy Laboratory and Sandia National Laboratories. It is part of the ExaWind modeling and simulation environment [23], built on top of the AmRex library [24]. AMR-Wind solves the three-dimensional incompressible Navier–Stokes equations in a spatially filtered resolved-scale formulation and employs a subgridscale model for smaller eddy dynamics. Furthermore, this works uses the available coupling between AMR-Wind and OpenFAST. The turbine is simulated using the ALM to accurately simulate the effect of individual blade pitching on the flow field.

The LES setup, illustrated in Figure 1, was designed so that the turbine wake can be examined without external disturbances such as the ground effect, gravitational force, or the turbine tower, which is crucial for its representation through an axisymmetrical velocity deficit model. All simulations used for the model calibration described in Section IV were conducted for a free-stream wind speed of $8\,\mathrm{ms}^{-1}$ and an ambient turbulence intensity of $TI_a = 4\%$. Further simulations for the model validation were performed for a wind speed of $9\,\mathrm{ms}^{-1}$ and an ambient turbulence intensity of $TI_a = 5.7\%$

The domain was discretized into cells of 10 m length with a single refinement around the turbine leading in 56 cells per diameter, starting $2D$ upstream and extending $5D$ downstream with respective $2D$ spacing into the lateral directions. All simulations were conducted with a time step of $\Delta t = 0.05s$. To isolate the influence of the wake from any boundary layer interactions, all simulations were conducted without shear and a slip boundary condition was applied at the lateral boundaries in agreement with [11]. The inlet features a constant velocity overlaid with fluctuations derived from a precomputed synthetic turbulence field generated with TurbSim [21]. The synthetic turbulence fluctuations are

introduced through a 2-dimensional plane.

The control signals for the helix approach were implemented using the reference open-source controller (ROSCO) toolbox for wind turbine applications [25]. To create the helical shape of the wake, slowly varying tilt and yaw signals are imposed on the turbine. These signals are designed in a non-rotating reference frame and then translated to the rotating reference frame by using the Multi-Blade Coordinate (MBC) transformation [26]. For further information on the MBC transformation of the helix, the reader is referred to [5].

IV. Model Calibration and Validation through High Fidelity Model

To capture the time-averaged flow field of the helix approach, the calibration parameters (b_s, c_s, b_f, c_f) of the surrogate model described in Section II were calibrated on flow field data of a single turbine operating under helix actuation in uniform inflow conditions. Note that the calibration parameter a_f was left at its initial value to maintain the super-Gaussian order as described in [12].

A. Wake model calibration

The following section outlines the step-by-step procedure used to calibrate the surrogate model with the LES data:

1) The extracted flow slices, containing of 560×280 points with a time resolution of 1s, from the high-fidelity simulations are time-averaged over 10 helix periods according to $T_{1P} = \frac{1}{f}$ with f denoting the helix actuation frequency. The different obtained time-averaged slices (xy-plane, xz-plane, and two diagonal cross-stream planes) are then again averaged to form one slice that is representative for the axisymmetric flow field.
2) The axisymmetric flow field is recreated in the surrogate model, using the same domain specifications as in the extracted high-fidelity slices. The turbine model used in the LES is recreated the pywake framework, using power and thrust coefficient curves obtained via OpenFAST simulations.
3) A cost function is set up in which the absolute error between the flow field data from AMR-wind and the predicted PyWake flow field is minimized for the arguments $\psi = [b_s, c_s, b_f, c_f]$, as:

$$\psi_{opt} = \arg\min_{\psi} \sum_{i=1}^{N} |v_{LES,i} - v_{model,i}| \,. \qquad (6)$$

Note that the calibration parameter a_s is kept constant at its predefined value of 0.17. The parameter describes the scaling of the characteristic wake width σ with changing ambient turbulent intensity TI_a. For a correct determination of a_s, several simulations with varying TI_a values would need to be conducted which will be conducted in the future. Therefore, the change of σ with TI_a is assumed to be constant for each simulation.

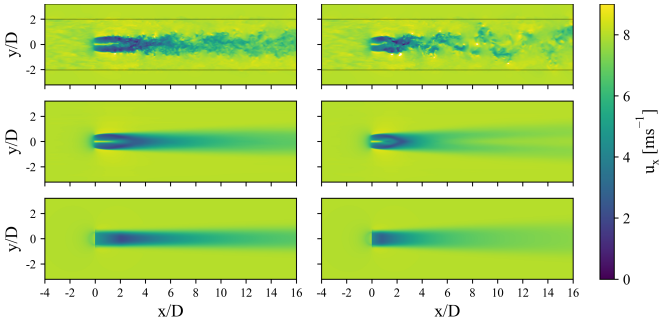

Fig. 2: Results of the calibration procedure for baseline operation (left side) and helix operation (right side). The uppermost row shows an instantaneous snapshot at $t = 2000s$ of the xy-plane. The black lines denote the lateral width of the turbulent flow. The second row shows the time-averaged axisymmetric velocity field. Finally, the third row shows the calibrated surrogate model.

B. Calibration Results

The methodology outlined in Section II was implemented in Python, utilizing a parallelized constrained genetic algorithm (GA). The solutions with the highest 20 fitness values were further averaged to find a set of parameters that was used for the final model. The GA was developed using the open-source *pygad* library [27]. The resulting optimal parameters, denoted as ψ_{opt}, are presented in Table I. A consistent trend in the calibrated parameters across varying helix amplitudes suggests that the optimization has not been overfitted to any single flow field.

TABLE I: Calibrated parameters with constant $a_s = 0.17$ for different pitch angle amplitudes of the helix approach.

	b_s	c_s	b_f	c_f
Baseline	0.020	0.202	-1.130	2.767
Helix (1°)	0.031	0.191	-2.570	2.983
Helix (3°)	0.047	0.189	-2.518	3.128
Helix (5°)	0.054	0.215	-0.775	2.536

When studying the visual results of the calibration procedure in Figure 2, it can be observed that the helix method shows a faster wake recovery and a more pronounced wake spreading when compared to the baseline case, which is well captured by the tuned surrogate model. However, the time-averaged velocity field also shows a double Gaussian velocity deficit, which is especially pronounced in the far wake region that is not well-captured by the surrogate model. This is expected, as the model was originally developed for baseline operation and thus has limitations in accurately representing the subtleties in the velocity field of a helical-perturbed wake.

C. Validation Results

Due to the computational cost of running an ALM-LES simulation for an entire wind farm, validation was performed using a single turbine LES simulation under different ambient conditions. Specifically, the model was tested at a higher

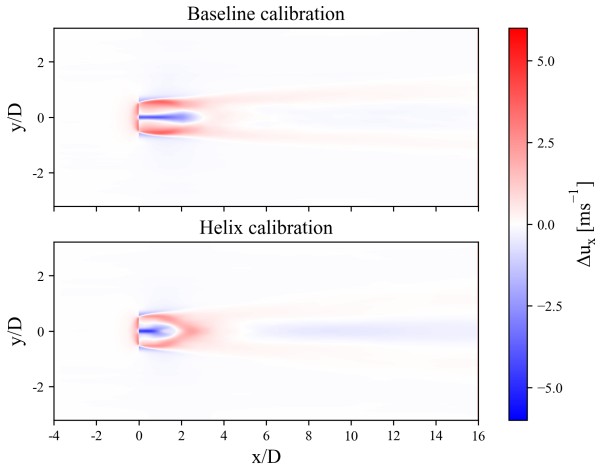

Fig. 3: Error of the calibrated model in different ambient conditions. The red colour shows an overestimation of the wind speed while the blue colour shows an underestimation.

wind speed of $9\,\mathrm{ms}^{-1}1$ and an increased ambient turbulence intensity of $TI_a = 5.7\%$.

The visual comparison between the calibrated model and the simulation is shown in Figure 3. In general, the flow field demonstrates good agreement with the calibrated model, particularly in the mid- and far-wake regions. However, larger discrepancies are observed in the near-wake region. For the helix calibration, the limitations of the surrogate model are apparent, as indicated by the underestimation of the velocity deficit in the center of the wake, which stems from a mismatch in the shaping function used to model the velocity deficit.

V. Case Study

The lower-left corner of the Hollandse Kust Noord (HKN) wind farm was selected as the reference site for this study. It is situated in the North Sea close to the Dutch coastline and gives a good reference for the next generation of offshore wind farms in the North Sea. The turbine coordinates were estimated using data from [28] and scaled according to the turbine diameter of $283.2\,\mathrm{m}$. Figure 4 compares the individual power output within the simulated farm under baseline operation, wake steering, and helix control for a wind speed of $8\,\mathrm{ms}^{-1}$ and an ambient turbulence intensity of $TI_a = 4\%$ for the wind direction of 201°, which is particularly important as it exhibits the highest wake losses observed for any wind direction. This angle was selected because it leads to a significant degree of wake overlap between the turbines, which can substantially impact power output and increase turbine fatigue. High wake overlap conditions, such as those seen for this wind direction, are of particular importance for operational optimization and turbine layout design.

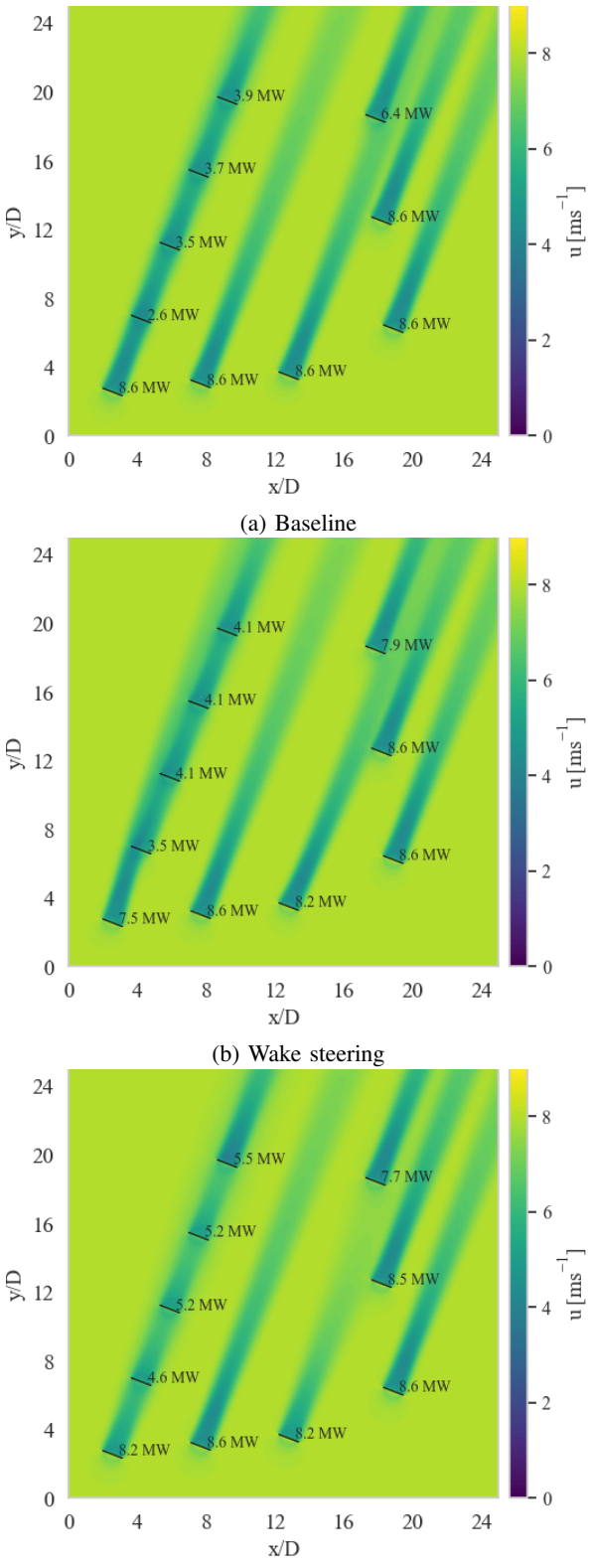

(a) Baseline

(b) Wake steering

(c) Helix

Fig. 4: Flow field at hub height ($170m$) of all Turbines for wind speed $8\,\mathrm{ms}^{-1}$ and $TI_a = 4\%$ for baseline operation (a), wake steering operation (b), and helix operation (c) for wind direction 201°.

A. Baseline case

Figure 4a illustrates the performance of all turbines operating in a conventional greedy mode. As expected, the front row of turbines achieves the maximum possible power output under the given ambient conditions. However, turbines located in the wake of others experience significant power reductions, with the most pronounced drop reaching up to 69.7% in the lower-left cluster. This wake-induced performance loss underscores the impact of wake interactions on downstream turbines. Overall, the total power output of the farm under these conditions is 63.1 MW.

B. Wake steering

To simulate the wake steering case, we used the baseline calibration of the surrogate wake model in combination with the wake redirection model from [16]. The yaw angles for the wake steering case were optimized, using a serial refinement approach following [29]. Given a set of possible yaw angles with 1° increments ranging from -20° to 20°, the yaw angle of each turbine was varied from the upstream to the downstream direction to maximize the cumulative power of the farm, formulated as:

$$\gamma_{opt_n} = \arg\max_{\gamma_n} \sum_{i=1}^{N} P_i. \tag{7}$$

This process was repeated for each individual wind direction. When studying Figure 4b, it becomes obvious that the most upstream turbine in the cluster on the left side experiences power losses due to the inclined inflow. However, all other turbines in its wake experience power gains, leading to a total power output of 65.2 MW, which is an increase of 3.03%.

C. Helix approach

Figure 4c shows the wind farm operating under helix actuation, with the pitch angles of the surrogate helix amplitude optimized, using an optimisation algorithm, following the serial refinement approach in Section V-B. Based on the given wind direction, the helix amplitudes of the upstream turbine were adjusted along the streamwise direction, and the total farm power output was compared to the baseline operation.The results show that helix operation was consistently selected whenever a downstream turbine was affected by the wake of the preceding turbine. In every case, the algorithm selected the highest possible helix amplitude of 5°, likely because the power losses associated with helical actuation were minimal in comparison to the downstream gains. However, it is important to note that this surrogate model focuses solely on maximizing power output. Since helix operation increases turbine loading, a different optimization algorithm considering structural loads might select lower amplitudes to balance power generation with operational stress. The total farm output in this case amounts to 70.3 MW which is a 11.4% gain in comparison to the baseline case and a 7.82% gain compared to wake steering.

D. Comparison

When studying the first turbine in the cluster on the left side in Figure 4c, the reduction in power is less pronounced than in Figure 4b, while the power production of the overall array shows a higher increase. However, the third turbine in the array shows a smaller power output than in the wake steering case. Another interesting effect can be seen when studying the interaction between the 4 turbines on the right side of the plot. In this cluster, wake steering results in a higher cumulative power production. Since the yaw misalignment of the upstream turbine is relatively small, its power production reduction is the same as for the helix actuation. However, the gain of the downstream turbine surpasses the gain from the helix case, resulting in a higher effectiveness of wake steering in this scenario. This can be partially explained by the relatively large downstream distance between the two turbines, which pronounces wake steering effects since the wake deflection has a larger area for its development.

Figure 5 illustrates the total farm power output as a function of wind direction. A dip in the upper plot indicates a wind direction with a high amount of wake losses. Respectively, the lower plot indicates that the relative power gains with wind farm control increase strongly during these periods. When comparing the performance of helix actuation and wake steering to baseline operation, they initially appear to provide similar gains. However, a closer examination of the normalized power output reveals distinct differences between the two under varying conditions. Helix actuation tends to outperform wake steering, particularly in scenarios where a significant number of turbines are directly aligned in the wake. In contrast, wake steering proves more effective when the wind direction is slightly misaligned with the turbine arrays, allowing for better optimization in these conditions. Looking at the power production in comparison to baseline operation, Wake steering achieves a higher maximum power gain of 12.5%, whereas helix operation reaches a maximum gain of 11.9%.

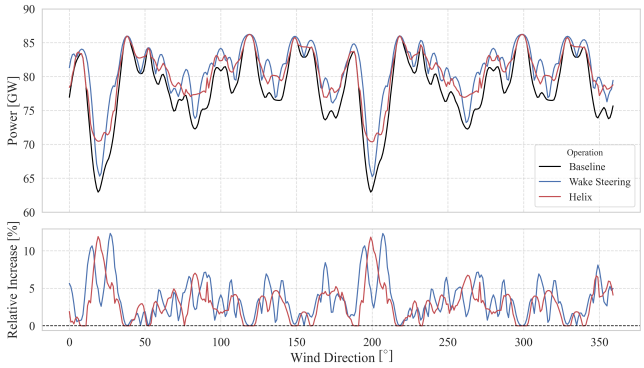

Fig. 5: Total farm power per wind direction. The upper plot shows the overall power output of baseline operation, optimized wake steering operation, and optimized helix operation. The bottom plot shows both, wake steering and helical actuation normalized with the baseline case.

VI. Conclusions

This study has shown that active wake control can significantly improve the power production and therefore performance of a wind farm. Especially for wind directions causing high wake losses, active wake control can improve energy harvest significantly by up to almost 12%. We demonstrated that the helix control is able to outperform wake steering when full turbine wake overlaps occur in an array. Wake steering on the other hand proves more effective in situations with partial wake overlap or increased downstream distance. Furthermore, a novel calibration methodology was developed and presented which facilitates the tuning procedure of engineering wake models through LES data.

Building on these findings, future research in wind farm wake control could focus on combining these techniques to exploit the benefits of each to further increase power generation. By tailoring wake control methods to specific wind conditions and wake interactions, there is significant potential to further enhance overall energy yield across the farm.

ACKNOWLEDGMENT

This work has been supported by the SUDOCO project, which receives the funding from the European Union's Horizon Europe Programme under the grant No. 101122256. The authors acknowledge the use of computational resources of the DelftBlue supercomputer, provided by Delft High Performance Computing Centre (https://www.tudelft.nl/dhpc).

References

[1] J. Meyers, C. Bottasso, K. Dykes, P. Fleming, P. Gebraad, G. Giebel, T. Göçmen, and J. W. van Wingerden, "Wind farm flow control: prospects and challenges," *Wind Energy Science*, vol. 7, no. 6, pp. 2271–2306, 2022. [Online]. Available: https://wes.copernicus.org/articles/7/2271/2022/

[2] M. F. Howland, S. K. Lele, and J. O. Dabiri, "Wind farm power optimization through wake steering," *Proceedings of the National Academy of Sciences*, vol. 116, no. 29, pp. 14 495–14 500, 2019.

[3] E. Simley, P. Fleming, and J. King, "Design and analysis of a wake steering controller with wind direction variability," *Wind Energy Science*, vol. 5, no. 2, pp. 451–468, 2020. [Online]. Available: https://wes.copernicus.org/articles/5/451/2020/

[4] P. Fleming, J. Annoni, J. J. Shah, L. Wang, S. Ananthan, Z. Zhang, K. Hutchings, P. Wang, W. Chen, and L. Chen, "Field test of wake steering at an offshore wind farm," *Wind Energy Science*, vol. 2, no. 1, pp. 229–239, 2017. [Online]. Available: https://wes.copernicus.org/articles/2/229/2017/

[5] J. A. Frederik, B. M. Doekemeijer, S. P. Mulders, and J. W. van Wingerden, "The helix approach: Using dynamic individual pitch control to enhance wake mixing in wind farms," *Wind Energy*, vol. 23, no. 8, pp. 1739–1751, 2020.

[6] D. Van der Hoek, J. Frederik, M. Huang, F. Scarano, C. Simao Ferreira, and J. W. van Wingerden, "Experimental analysis of the effect of dynamic induction control on a wind turbine wake," *Wind Energy Science*, vol. 7, no. 3, pp. 1305–1320, 2022.

[7] E. A. Bossanyi, "Individual blade pitch control for load reduction," *Wind Energy: An International Journal for Progress and Applications in Wind Power Conversion Technology*, vol. 6, no. 2, pp. 119–128, 2003.

[8] K. Selvam, S. Kanev, J. W. van Wingerden, T. van Engelen, and M. Verhaegen, "Feedback–feedforward individual pitch control for wind turbine load reduction," *International Journal of Robust and Nonlinear Control: IFAC-Affiliated Journal*, vol. 19, no. 1, pp. 72–91, 2009.

[9] A. A. Van Vondelen, S. T. Navalkar, D. R. Kerssemakers, and J. W. Van Wingerden, "Enhanced wake mixing in wind farms using the helix approach: A loads sensitivity study," in *2023 American Control Conference (ACC)*. IEEE, 2023, pp. 831–836.

[10] E. Taschner, A. van Vondelen, R. Verzijlbergh, and J. W. van Wingerden, "On the performance of the helix wind farm control approach in the conventionally neutral atmospheric boundary layer," *Journal of Physics: Conference Series*, vol. 2505, no. 1, p. 012006, 5 2023. [Online]. Available: https://dx.doi.org/10.1088/1742-6596/2505/1/012006

[11] H. Korb, H. Asmuth, and S. Ivanell, "The characteristics of helically deflected wind turbine wakes," *Journal of Fluid Mechanics*, vol. 965, p. A2, 2023.

[12] F. Blondel and M. Cathelain, "An alternative form of the super-gaussian wind turbine wake model," *Wind Energy Science*, vol. 5, no. 3, p. 1225–1236, Sep. 2020.

[13] E. Branlard and M. Gaunaa, "Cylindrical vortex wake model: right cylinder," *Wind Energy*, vol. 18, no. 11, pp. 1973–1987, 2015. [Online]. Available: https://onlinelibrary.wiley.com/doi/abs/10.1002/we.1800

[14] S. Frandsen, "Turbulence and turbulence-generated structural loading in wind turbine clusters," Ph.D. dissertation, Denmark Technical University, 2007, risø-R-1188(EN).

[15] NREL, "Floris: A controls-oriented engineering wake model," https://github.com/nrel/floris, 2024, version 4.1.1, BSD-3-Clause License.

[16] Á. Jiménez, A. Crespo, and E. Migoya, "Application of a les technique to characterize the wake deflection of a wind turbine in yaw," *Wind energy*, vol. 13, no. 6, pp. 559–572, 2010.

[17] M. Abramowitz and I. Stegun, "Handbook of mathematical functions pover," *New York*, 1970.

[18] M. M. P. et al., "Pywake 2.5.0: An open-source wind farm simulation tool," 2 2023. [Online]. Available: https://gitlab.windenergy.dtu.dk/TOPFARM/PyWake

[19] F. Zahle, A. Barlas, K. Lønbæk, P. Bortolotti, D. Zalkind, L. Wang, C. Labuschagne, L. Sethuraman, and G. Barter, "Definition of the IEA Wind 22-Megawatt Offshore Reference Wind Turbine," Technical University of Denmark, International Energy Agency, Tech. Rep. DTU Wind Report E-0243, https://doi.org/10.11581/DTU.00000317, 2024.

[20] National Renewable Energy Laboratory, "OpenFAST: Open-source wind turbine simulation tool," https://github.com/OpenFAST/openfast, 2024, accessed: 2024-09-26.

[21] N. D. Kelley and B. J. Jonkman, "Overview of the turbsim stochastic inflow turbulence simulator: Version 1.21 (revised february 1, 2001)," 4 2007. [Online]. Available: https://www.osti.gov/biblio/903073

[22] M. Bastankhah and F. Porté-Agel, "A new analytical model for wind-turbine wakes," *Renewable energy*, vol. 70, pp. 116–123, 2014.

[23] A. Sharma, M. J. Brazell, G. Vijayakumar, S. Ananthan, L. Cheung, N. deVelder, M. T. Henry de Frahan, N. Matula, P. Mullowney, J. Rood, P. Sakievich, A. Almgren, P. S. Crozier, and M. Sprague, "Exawind: Open-source cfd for hybrid-rans/les geometry-resolved wind turbine simulations in atmospheric flows," *Wind Energy*, vol. 27, no. 3, pp. 225–257, 2024. [Online]. Available: https://onlinelibrary-wiley-com.tudelft.idm.oclc.org/doi/abs/10.1002/we.2886

[24] W. Zhang, A. Almgren, V. Beckner, J. Bell, J. Blaschke, C. Chan, M. Day, B. Friesen, K. Gott, D. Graves, M. Katz, A. Myers, T. Nguyen, A. Nonaka, M. Rosso, S. Williams, and M. Zingale, "Amrex: a framework for block-structured adaptive mesh refinement," *Journal of Open Source Software*, vol. 4, no. 37, p. 1370, May 2019.

[25] NREL, "ROSCO. Version 2.4.1," 2021. [Online]. Available: https://github.com/NREL/ROSCO

[26] G. Bir, "Multi-blade coordinate transformation and its application to wind turbine analysis," in *46th AIAA aerospace sciences meeting and exhibit*, 2008, p. 1300.

[27] A. F. Gad, "Pygad: An intuitive genetic algorithm python library," *Multimedia Tools and Applications*, pp. 1–14, 2023.

[28] 4C Offshore, "Global offshore renewable map," https://map.4coffshore.com/offshorewind/, 2024, accessed: 2024-09-25.

[29] P. A. Fleming, A. P. Stanley, C. J. Bay, J. King, E. Simley, B. M. Doekemeijer, and R. Mudafort, "Serial-refine method for fast wake-steering yaw optimization," in *Journal of Physics: Conference Series*, vol. 2265, no. 3. IOP Publishing, 2022, p. 032109.